Influence of spatially segregated IP_3-producing pathways on spike generation and transmitter release in Purkinje cell axons

Laura C. Gomez[a,b], Shin-ya Kawaguchi[c], Thibault Collin[a], Abdelali Jalil[a], Maria del Pilar Gomez[a,d], Enrico Nasi[a,e], Alain Marty[a], and Isabel Llano[a,1]

[a]Saints Pères Paris Institute for the Neurosciences, Université Paris Descartes, 75006 Paris, France; [b]Department of Physics and Astronomy, University of British Columbia, Vancouver V6T1Z1, BC, Canada; [c]Department of Biophysics, Graduate School of Science, Kyoto University, 606-8502 Kyoto, Japan; [d]Departamento de Biología, Universidad Nacional de Colombia, Bogotá 111321, Colombia; and [e]Instituto de Genética, Universidad Nacional de Colombia, Bogotá 111321, Colombia

Edited by Kurt G. Beam, University of Colorado Denver, Anschutz Medical Campus, Aurora, CO, and approved March 20, 2020 (received for review January 13, 2020)

It has been known for a long time that inositol-trisphosphate (IP_3) receptors are present in the axon of certain types of mammalian neurons, but their functional role has remained unexplored. Here we show that localized photolysis of IP_3 induces spatially constrained calcium rises in Purkinje cell axons. Confocal immunohistology reveals that the axon initial segment (AIS), as well as terminals onto deep cerebellar cells, express specific subtypes of Gα/q and phospholipase C (PLC) molecules, together with the upstream purinergic receptor P2Y1. By contrast, intermediate parts of the axon express another set of Gα/q and PLC molecules, indicating two spatially segregated signaling cascades linked to IP_3 generation. This prompted a search for distinct actions of IP_3 in different parts of Purkinje cell axons. In the AIS, we found that local applications of the specific P2Y1R agonist MRS2365 led to calcium elevation, and that IP_3 photolysis led to inhibition of action potential firing. In synaptic terminals on deep cerebellar nuclei neurons, we found that photolysis of both IP_3 and ATP led to GABA release. We propose that axonal IP_3 receptors can inhibit action potential firing and increase neurotransmitter release, and that these effects are likely controlled by purinergic receptors. Altogether our results suggest a rich and diverse functional role of IP_3 receptors in axons of mammalian neurons.

calcium | IP_3 | cerebellum | excitability | axon

In mammalian neurons, the endoplasmic reticulum (ER) is not restricted to the somatodendritic compartment, but it extends also in the axon, up to the most distal presynaptic terminals (1). A number of studies have demonstrated the implication of ER-associated intracellular Ca^{2+} stores in axonal signaling and in the control of neurotransmitter release. Spontaneous, local Ca^{2+} elevations elicited by Ca^{2+}-induced Ca^{2+} release (CICR) were reported in axons of interneurons of cerebellar slices (2, 3) and of cultured hippocampal neurons (4) and are thought to participate in the control of transmitter release. Recently, ER Ca^{2+} levels were shown to regulate transmitter release (5). The ER membrane usually carries inositol 1,4,5-trisphosphate receptors (IP_3Rs) as well as ryanodine receptors (RyRs, reviewed in ref. 6). Whereas RyRs are sensitive to Ca^{2+} elevation, IP_3Rs are activated by phospholipase C (PLC)-driven IP_3 production (reviewed in ref. 7). The PLC-IP_3 pathway has been extensively studied in somatodendritic compartments, where it contributes to postsynaptic signaling and induces various forms of long-term synaptic plasticity (reviewed in ref. 8). The same pathway is also well documented in the luminal compartment of exocrine acinar cells, where it controls electrolyte secretion and exocytosis (9). Since the luminal end of exocrine acinar cells bears a deep-running resemblance to the axonal compartment of neurons, presumably reflecting a common ancestral design (10), it is plausible that IP_3Rs are likewise important for axonal function. If a functional PLC-IP_3 pathway exists in central presynaptic terminals, it could offer a way to activate neurotransmitter release using presynaptic intracellular Ca^{2+} stores that would be distinct from RyR-dependent exocytosis. In addition, IP_3Rs could have a functional role outside the terminal region, since recent studies suggest structural and functional differences between various locations of central axons including the axon initial segment (AIS), paranodal regions, branch points, and axon collaterals (11–13). Surprisingly, such possible actions of IP_3Rs have not been investigated, and it is presently unknown whether axons of central neurons possess functional IP_3Rs.

Purkinje cells (PCs) offer an ideal model to study axonal IP_3Rs. These neurons contain a high level of IP_3Rs in addition to RyRs, and their implication in calcium signaling in the somatodendritic compartment has been well documented (14, 15, reviewed in refs. 8 and 16). Furthermore, IP_3Rs were observed in PC axons (17), but it is not known whether these receptors are able to mobilize Ca^{2+} from the ER. In PCs, action potentials (APs) produce significant Ca^{2+} elevation in the AIS (18) and in Ranvier nodes (19, 20), as well as in presynaptic terminals of axon collaterals (21–23). These Ca^{2+} rises are thought to regulate AP initiation (24), AP propagation (19, 20), and short-term synaptic plasticity (21, 22). Using local IP_3 delivery by focal photolysis of caged IP_3, we show that functional IP_3Rs are present in the entire

Significance

IP_3 receptors are well-documented regulators of intracellular calcium concentration, but their role in axons of central neurons remains unexplored. Here we show that IP_3 receptors are present throughout the axon of cerebellar Purkinje cells where their activation leads to calcium release from intracellular stores. We reveal distinct, sharply delimited signaling cascades leading to IP_3 production in the axon initial segment (AIS), in the more distal part of the axon, and in synaptic terminals. In the AIS, IP_3-induced calcium rises inhibit action potential generation, whereas similar signals in axonal terminals increase transmitter release. Metabotropic purinergic receptors appear to control the IP_3-driven cascade. Altogether, the results reveal potent actions of IP_3 in central axons, which are both diverse and spatially constrained.

Author contributions: S.-y.K., T.C., M.d.P.G., E.N., A.M., and I.Ll. designed research; L.C.G., S.-y.K., T.C., A.J., M.d.P.G., E.N., A.M., and I.Ll. performed research; L.C.G., S.-y.K., T.C., A.J., M.d.P.G., E.N., A.M., and I.Ll. analyzed data; and A.M. and I.Ll. wrote the paper with assistance from all authors.

The authors declare no competing interest.

This article is a PNAS Direct Submission.

[1]To whom correspondence may be addressed. Email: isabel.llano@parisdescartes.fr.

This article contains supporting information online at https://www.pnas.org/lookup/suppl/doi:10.1073/pnas.2000148117/-/DCSupplemental.

First published May 1, 2020.

axon. We further reveal different IP_3-producing pathways in different axon regions using immunocytochemistry. Finally, we demonstrate diverse consequences of IP_3R activation depending on IP_3R localization: while IP_3R activation in terminals leads to neurotransmitter release, IP_3R activation in the AIS inhibits AP firing.

Results

PC Axon Staining with IP_3R Antibody. To investigate the spatial distribution of IP_3R type I, anti-IP_3R-I antibodies were tested in sagittal cerebellar slices of both rats and mice at ages ranging from postnatal day 12 (PN12) to PN45. As illustrated in Fig. 1*A* for a rat at PN16 (*Left*), prominent staining was obtained in the somatodendritic compartment of PCs as well as in their axons. IP_3R-I staining was present throughout the entire axonal arborization, including the axonal projections to the deep cerebellar nuclei (DCN), where structures resembling synaptic boutons over DCN somata could be visualized (Fig. 1*D*). No label was present with antibodies preadsorbed to the immunogenic peptide (Fig. 1 *A*, *Right*). A similar pattern of IP_3R-I expression was observed in adult rats (example in Fig. 1*B* at PN31), indicating that the presence of IP_3Rs along the axon is not a transient developmental phenomenon. IP_3R expression was similar in rats and in mice. Comparing Fig. 1*C* (staining in mouse) to Fig. 1*A* (staining in rat) shows that IP_3R-I expression in the granule cell layer was similar in rats and in mice. Expression was confined to the axons of PCs, as ascertained by colocalization with the well-known PC marker calbindin (Fig. 1*C*).

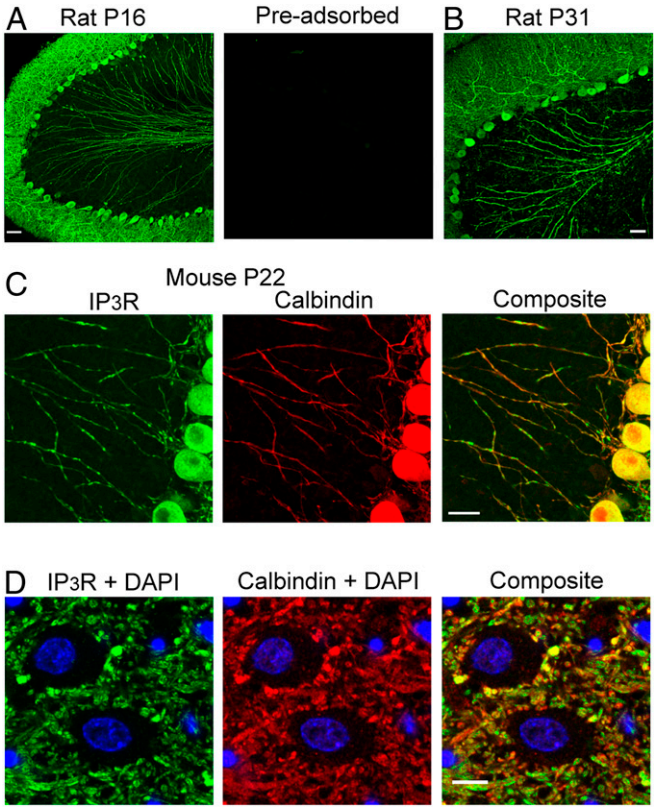

Fig. 1. IP_3R expression in PCs includes axons. (*A* and *B*) Low-magnification (20×) confocal immunofluorescence images of rat sagittal cerebellar slices stained with an antibody targeting type-I IP_3Rs. Slices exposed to the same antibody preincubated with the immunogenic peptide were completely devoid of marker (*A*, *Right*). IP_3R immunofluorescence, which is prominent in the somatodendritic compartment of PCs, clearly extends to the axons. Similar results were observed with young (*A*) and with adult rats (*B*). (Scale bar, 50 μm.) (*C*) The same expression pattern was present in mice; the assay included calbindin colabeling to highlight the colocalization of the two proteins along the axons. (Magnification, 63×.) (Scale bar, 20 μm.) (*D*) Zoom on a small field in the DCN highlights the presence of IP_3R-I (*Left*) on synaptic-like boutons surrounding DCN somata, counterstained with DAPI. (*D*, *Middle*) PC axons and synaptic boutons labeled by calbindin. (*D*, *Right*) Composite for the three channels. (Scale bar, 5 μm.)

IP_3 Photolysis in PC Axons. To investigate whether axonal IP_3Rs were functional, we used localized IP_3 photolysis, as schematized in Fig. 2*A*. PCs were dialyzed with a K gluconate-based solution supplemented with the calcium probe Oregon Green 488 BAPTA-1 (OGB1) and caged IP_3. Two-photon laser scanning microscopy (2PLSM) was used to follow the PC axon as it courses through the granule cell layer (Fig. 2*B*). To elicit a local IP_3 rise, a short pulse of 405-nm laser excitation was delivered to a diffraction-limited spot in the axon (*Methods*). Such stimuli elicited local Ca_i responses, as shown in Fig. 2 *C* and *D* for two different regions of the PC axon illustrated in Fig. 2*B*. The first region is located at an axonal branch point (Fig. 2*C*), whereas the second region corresponds to presynaptic terminals formed by an axonal collateral that returns to the PC layer (Fig. 2*D*, these terminals outline the shape of a presumptive postsynaptic PC soma). In both cases, the calcium rises rapidly (time to peak: 20 to 40 ms) and returns to baseline with time constants of 0.6 to 1 s. A similar photolysis protocol was used to probe PC axons at various locations including the AIS (0 to 25 μm from the soma exit; see below), smooth axon segments excluding varicosities, axonal enlargements resembling varicosities, branch points, putative terminals, and on occasion stumps from axons that were cut during the slicing procedure. Group results from 47 experiments are summarized in Fig. 2*E*, where signals for peak Ca_i rises are plotted as a function of the distance from the axon exit at the soma level to the photolysis site and different symbols code for different axonal morphology and photolysis parameters (see Fig. 2*E* legend). The results reveal similar levels of responsiveness for all data groups, in accord with immunocytochemical results indicating widespread distribution of IP_3Rs in the axon domain. Nevertheless, the results also display a wide variability within each data group. They show a general downward trend for large distances, possibly reflecting limited diffusion of the IP_3 cage during whole-cell recording (WCR). In addition, although care was taken to select PCs whose axons were traveling within 40 μm from the slice surface, some of the scatter may reflect depth differences of the imaged axon spots, because photolysis efficiency decreases strongly as the 405 nm light travels in the tissue (25). Despite the variability across axonal sites, Ca_i rises at a given spot were consistent across repetitions.

We next examined the dependence of Ca_i responses on photolysis parameters (Fig. 3 *A* and *B*, representative of three experiments). For pulses in the low millisecond range, the peak response amplitude increases in a sigmoid fashion with laser pulse intensity, while the latency and rise time are reduced (Fig. 3*A*, corresponding peak amplitudes are shown as black symbols in Fig. 3*B*). Changing the duration or intensity while maintaining the product of the two parameters constant does not affect the resulting Ca_i rise (Fig. 3*B*, compare black and red symbols). The curve saturated for larger stimuli (>1 ms*V), suggesting that such stimuli release a large fraction of the locally available IP_3, or alternatively, that Ca_i rises caused saturation of OGB1, as discussed below. A calibration procedure was carried out (*Methods*), suggesting that the 1 ms*V intensity, roughly corresponding to the half maximal effective concentration (EC_{50}) of the dose–response curve in Fig. 3*B*, reflects a local IP_3 concentration near 40 μM. These results are in line with earlier uncaging results performed in the somatodendritic compartment, that also indicate an apparent EC_{50} near 40 μM when using the low-affinity indicator furaptra (26). The low affinity of IP_3Rs for IP_3 in PCs compared to other cells is attributed to the association of IP_3R_1 receptors with the protein CA8 (27). The

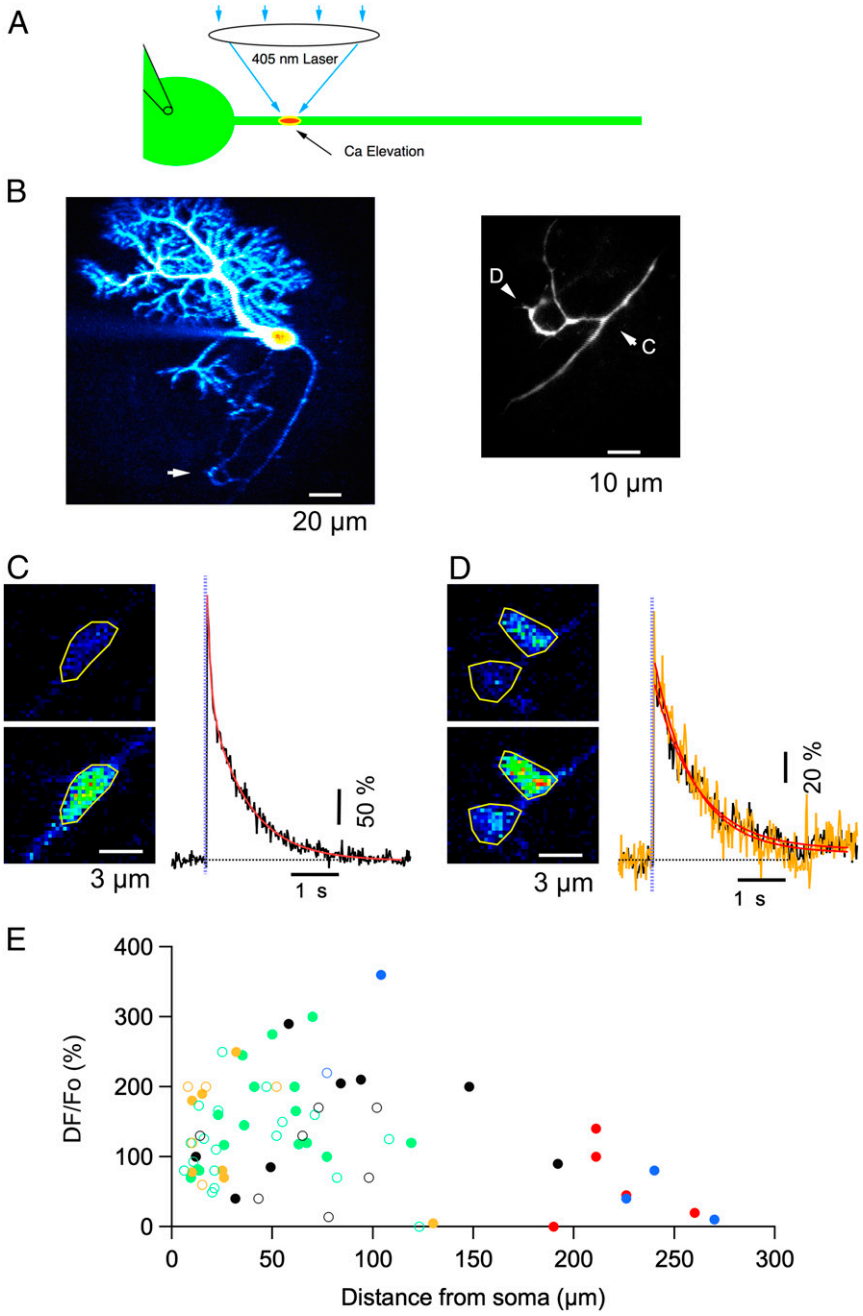

Fig. 2. Local photolysis reveals functional IP_3Rs along PC axons. (*A*) Schematics of the experimental paradigm: a patch-clamp pipette on the PC soma allows WCR and diffusion into the axon of the Ca probe OG1, of Alexa 594 and of caged IP_3. A 405-nm laser beam is directed to specific axonal locations and the ensuing fluorescence changes are monitored with 2PLSM. (*B*, *Left*) 2PLSM projection of Alexa 594 fluorescence in a PC with extensive dendritic and axonal arborizations. The expanded view on the *Right* corresponds to the region highlighted by the white arrow, which includes the first branching point and an axonal collateral that returns to make terminal-like boutons over another PC soma. Labeled arrowheads point to two subregions analyzed in *C* and *D* (respectively, a branch point and presynaptic terminals onto a presumptive postsynaptic PC soma). (*C*, *Left*) Images from a branch point taken at rest (*Upper*) and at the peak of the response to a photolysis pulse of 1-ms duration, 1-V amplitude (*Bottom*). (*C*, *Right*) Time course of the ensuing fluorescent rise on the ROI drawn on the peak image. The red trace corresponds to a double exponential fit with time constants and amplitude coefficients of 72 ms, 136% and 0.8 s, 237%. In this and subsequent figures the time of the laser pulse is indicated by purple vertical dots. (*D*) Similar to *C*, showing responses in presumptive synaptic terminals. Two ROIs are analyzed in this case (black and yellow traces on the *Right*), each corresponding to a putative terminal over the PC soma. In these structures, the decay was well approximated by a single exponential with time constants of 0.8 and 0.9 s for the two ROIs, respectively. (*E*) Pooled data on the peak Ca_i rises elicited by 2 ms*V (open circles) or 4 ms*V (closed circles) laser pulses at different axonal locations. Values are expressed as $\Delta F/F_o$ corresponding to $100*(F-F_o)/(F_o-B)$ (*Methods*). The color codes for the morphology are as follows: green for smooth axon, blue for branching points, black for axonal enlargements, red for terminal-like structures, and yellow for axonal stumps.

present finding of low-affinity IP_3 responses in the axon is consistent with the earlier finding that CA8 is expressed in the axons as well as in the somatodendritic compartment of PCs (27). Next we questioned the range of Ca^{2+} concentrations reached by IP_3 uncaging. Since in the experiments of Fig. 3 we used an indicator with high affinity (OGB1), we performed additional experiments with the calcium indicator fura 6F, that has a lower affinity for Ca^{2+} than OGB1 (respective K_d values, 5 µM and

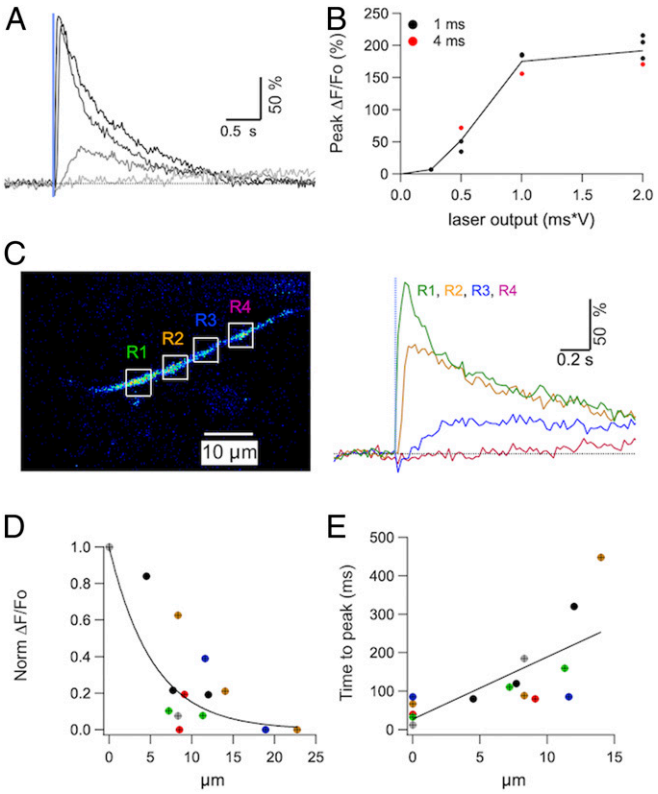

Fig. 3. Dependence of IP_3-evoked Ca_i rises on space and photolysis parameters. (*A*) Ca_i rises evoked in an axonal varicosity by 1-ms laser pulses of amplitudes 0.25, 0.5, 1, and 2 V, showing that peak amplitude and onset speed increase as a function of laser intensity. (*B*) The relation between peak Ca_i rise and laser output (the product of laser intensity with pulse duration) for the experiment shown in *B* is displayed for laser pulse durations of 1 ms (black) and 4 ms (red). The results are fit with a single relation (line) showing supralinearity at low output values and saturation at high output values. (*C*, *Left*) Multiple ROI two-photon scan was performed as detailed in *Methods* to probe for the diffusional properties of the IP_3-evoked Ca_i rise. In this example, four axonal regions (R1 to R4) outlined by white boxes were scanned and the 405-nm laser was centered close to the right edge of R1. (*C*, *Right*) Both signal amplitude and onset speed decrease with distance from the targeted axonal site. (*D*) Data from six experiments (each represented by a different color) showing the dependence of peak Ca_i rise on distance from the photolysis site. Peak ΔF/Fo values were normalized to the value at the targeted site (x = 0 µm). The black line corresponds to the fit of the data by a single exponential function with a space constant of 5.3 µm. (*E*) Relation between time to peak and distance for the same data set as in *D*. The black line corresponds to the fit by a linear function. The slope of this line, 16.1 ms/µm, is different from 0 (Pearson's coefficient 0.735, $n = 16$; $P < 0.01$), indicating a significant positive correlation between distance and rise time.

0.2 µM). With two-photon illumination, fura 6F signaled Ca^{2+} concentration increases as fluorescence decreases. We found responses of −44.3 ± 7.6% (five axonal spots from three PCs) for a stimulation strength of 4 ms*V (*SI Appendix*, Fig. S1). Since saturating Ca^{2+} concentration increases (obtained with prolonged AP trains at high frequency) essentially abolished the fura 6F fluorescence, a 44% decrease roughly corresponds to a Ca^{2+} concentration equal to the K_d of fura 6F, that is 5 µM. These results indicate that IP_3R-induced Ca^{2+} responses reach 5 µM or more following strong uncaging stimulations. Because OGB1 is close to saturation at such concentrations, the results also indicate that dye saturation contributes to the saturation of the dose–response curve in Fig. 3*B*. Altogether, the two main features of the dose–response curve of Fig. 3*B* (sigmoid rise at low intensity and saturation at high intensity) are consistent with earlier results obtained by IP_3 photolysis in the somatodendritic compartment of PCs using the low-affinity indicator furaptra (26).

To investigate the spatial spread of IP_3-induced Ca_i signals, we analyzed Ca_i rises in axonal locations adjacent to that targeted by the laser spot. For this purpose, we used a special scanning protocol (*Methods*) that rapidly switched between user-defined regions of interest (ROIs) during the IP_3-induced response. In the example shown we chose a first ROI at the site of IP_3 release, and several additional ROIs located at various distances along the axon. The result, illustrated in Fig. 3*C*, indicates that Ca_i signals induced by IP_3 photolysis are spatially constrained near the site of IP_3 production. Data pooled from six experiments show that the peak Ca_i response decreases rapidly with distance from the photolysis site (Fig. 3*D*), whereas the onset time increases with distance (Fig. 3*E*). We next asked whether IP_3-evoked Ca_i transients are influenced by ryanodine receptors. In PC soma and dendrites, ryanodine inhibits IP_3-evoked Ca_i transients (28). This effect likely reflects the emptying of IP_3-sensitive stores following activation of ryanodine receptors, indicating that IP_3Rs and ryanodine receptors are located on common structures (28). To examine whether the same holds true in the axon, an axonal spot was exposed to repeated photolysis pulses, spaced at 3- to 5-min intervals, and after reaching a stable baseline the CICR antagonist ryanodine was added to the bath solution. In the example shown in *SI Appendix*, Fig. S2, this abolished the Ca_i rises. The extent of inhibition varied among experiments and on average, ryanodine reduced the photolysis-evoked Ca_i signals to approximately half their control value, with a statistically significant reduction of the response (mean ratio in ryanodine vs. control: 0.51 ± 0.12, $n = 9$, $P = 0.01$; see *SI Appendix*, Fig. S2). This indicates that ryanodine receptors and IP_3Rs both contribute to Ca_i rises originating from axonal ER, and that the two types of receptors are located on common structures.

Upstream Signaling Cascades Leading to IP_3 Production. The functionality of axonal IP_3Rs prompts the question of local availability of the machinery to engage them. Expression of different phosphoinositide-specific phospholipases (PLCs) is well documented in the cerebellar cortex of mammals, mostly in the somatodendritic compartment of PCs, but the presence of at least one type of PLC has also been reported in the axons (29). Two broad possibilities were considered for endogenous IP_3 production: 1) as the result of the axon's own activity and 2) in response to an external stimulus. The first possibility could occur if AP-induced local Ca_i changes recruit one of the Ca-dependent PLCs known to express in the cerebellum, namely, PLC-δ3 (30) and PLC-η1 (31, 32). However, functional consequences of manipulating the PLC-δ3 gene appear restricted to granule cells in the cerebellum (30), and an xPLC-δ3 antibody failed to stain PCs. In addition, while we found staining for a xPLC-η1 antibody in PC somata and dendrites, PC axons failed to display any staining (*SI Appendix*, Fig. S3). Therefore, neither PLC-δ3 nor PLC-η1 appeared as likely candidates. The second possibility could involve a PLC of the β-class, which are activated by "q"-type G proteins. We first tested antibodies targeting the classical $G_{q/11}$, focusing on the somatic and axonal regions of PCs. As Fig. 4*A* illustrates, xG_q antibodies prominently label axons in the granule cell layer, corroborating previous findings (29); costaining with anti-calbindin antibodies confirmed that these originated from PCs. However, G_q labeling conspicuously spared the AIS, which is puzzling because IP_3Rs are present in that region (Fig. 1). We therefore explored other Gα proteins of the same subfamily. The human protein Gα16 (and its rodent ortholog Gα15) can activate all four types of PLC-β (33–36); although its expression levels in the brain are generally low (37), Gα16 could have a role at specific locations. As shown in Fig. 4*B*, xGα16 antibodies clearly decorated the proximal axons of PCs; colabeling assays revealed a striking colocalization with ankyrin G, identifying this zone as the AIS (38). The complementarity of the two types of Gα of the "q"

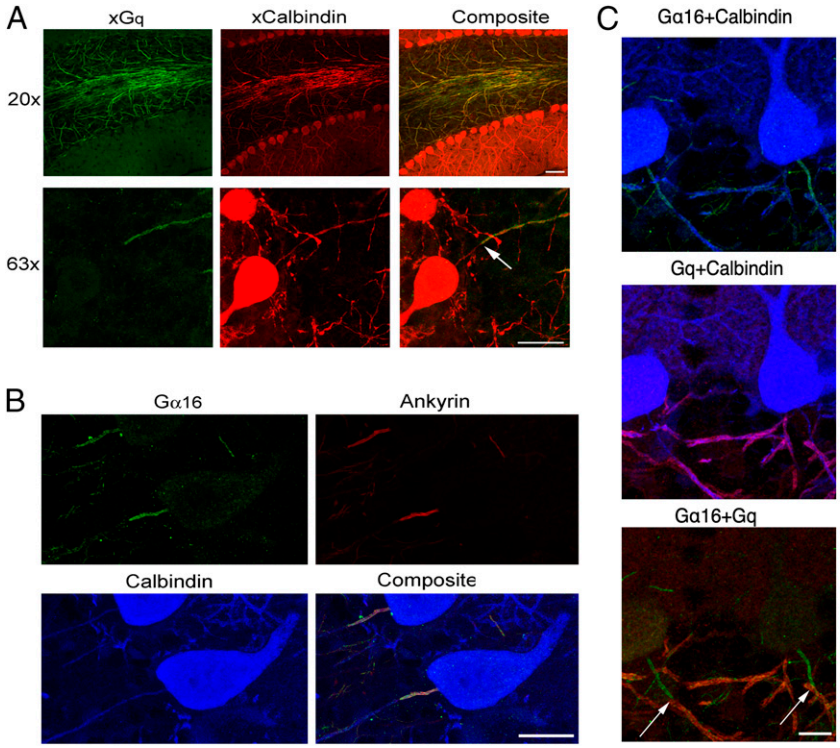

Fig. 4. Expression of G_q class proteins in PC axons. (*A*, *Top*) Low-magnification immunofluorescence images using an antibody that targets $G_{q/\alpha 11}$ (green) show prominent G_q labeling along axons in the granule cell layer and diffuse labeling in the molecular layer; colocalization with calbindin (red) indicates that the axons belong to PCs. (*A*, *Bottom*) High-magnification images reveal that axonal G_q expression starts >20 μm away from the soma, leaving an initial stretch devoid of label (arrow). (*B*) Anti-$G_{\alpha 15/\alpha 16}$ antibody stains the proximal segment of PC axons. The spatial pattern of $G_{\alpha 15/\alpha 16}$ expression (green) coincides with that of ankyrin G (red; blue: calbindin counterstain marking PC outline). (*C*) Triple staining with calbindin (blue), $G_{\alpha 15/\alpha 16}$ (green), and G_q (red) showing complementary expression of the two proteins: $G_{\alpha 15/\alpha 16}$ at the initial segment, followed thereafter with no gap or overlap, by G_q expression in the distal portion (transitions at arrows). (Scale bars: *A*, *Top*: 50 μm; all others: 20 μm.)

family was verified by simultaneous labeling with xGq and xGα16 antibodies: Fig. 4*C* shows that the axonal regions labeled by the two markers abut one another, with little or no overlap.

We next examined possible target enzymes of these G proteins, namely, β-type PLCs. Immunofluorescence assays with xPLC-β4, focusing on the Purkinje and granular layers, failed to reveal any axonal labeling; by contrast, as shown in Fig. 5, xPLC-β3 clearly marked axons—in addition to somata—of PCs, as confirmed by costaining with antibodies against the IP_3R (Fig. 5*A*) and calbindin (Fig. 5*C*). This corroborates observations in ref. 29. At the subcellular level, PLC-β3 accumulated in the axonal membrane, as highlighted by the fluorescence intensity profiles displayed in Fig. 5*B*, in contrast with the diffuse internal distribution of IP_3Rs, which is expected due to its association with the ER. As in the case of G_q, the initial part of the PC axon was devoid of the PLC-β3 label (Fig. 5*C*), which was baffling, given the expression of Gα16 in the AIS. We examined the other two forms of PLC-β (β1 and β2), which are not present at high levels in whole-cerebellum assays (39, 40), but could exhibit a restricted expression at specific locations. Indeed, while assays with xPLC-β1 were negative, xPLC-β2 antibodies specifically labeled PC AIS, colocalizing with ankyrin G (Fig. 5*D*) as shown for Gα15/α16 (Fig. 4*C*). Altogether, the AIS and the distal axon have each a distinctive set of the Gα/q-PLC pathway (Fig. 5*E*).

Downstream Effects of IP_3 in the Axon Initial Segment. The spatially distinct pattern for PLC and Gα/q proteins suggested that axonal IP_3Rs may have distinct functional roles at different axonal locations. In particular, our finding of a specific upstream signaling pathway leading to IP_3 production in the AIS led us to examine effects of photolytic release of IP_3 in this region of the axon.

The AIS is the site where the AP is generated and as such it is a pivotal excitability control point (11, 12). Ca_i rises could affect the balance of depolarization/hyperpolarization at the AIS by regulating Ca-sensitive channels, such as BK channels, as well as by regulating the opening probability of other voltage-gated ion channels. We hypothesized that IP_3-evoked Ca_i rises may alter the probability of producing an AP and we examined this possibility in current-clamp recordings. PCs were maintained at −77 to −79 mV by steady current injection in order to avoid spontaneous spiking and trains of 20 depolarizing current pulses (5-ms duration; pulse frequency: 50 Hz) were delivered at 1-min intervals. The current amplitude during these pulses was adjusted so that an AP was elicited in 35 to 45% of the pulses during each train. To probe for IP_3 effects, photolysis was induced before the 10th pulse in half of the trains, alternating with control trains. In this series of experiments, only PCs with axons that extended for more than 200 μm in the granule cell layer were studied, thus avoiding potential abnormal AP generation/propagation in axons with cut ends close to the AIS. A representative experiment is shown in Fig. 6. In control runs (no photolysis: Fig. 6*A1*), successful APs during the train led to a cumulative Ca_i rise in the AIS, with an average peak AP-evoked Ca_i rise of 64.1 ± 5.2% (n = 10). In interleaved photolysis runs (Fig. 6*A2*), IP_3 generated a fast-rising Ca_i component that added to the AP-evoked Ca_i rise, leading to a peak Ca_i value of 122.5 ± 15.4% (n = 10). To quantify the effect of photolysis on AP generation, we counted AP numbers for the first 9 pulses of the train as well as for the last 11 pulses of the train and calculated in each case the percentage change in AP numbers between control and photolysis runs. This spike number change was averaged over repetitions in individual recordings. The results from 15 experiments were divided in two groups, the "AIS" group which included all axonal spots located at less than 26-μm distance from the axon exit point (this value being based on ankyrin G labeling data) and the "distal" group which included all axonal spots located at distances larger than 30 μm from the exit. For the last 10 stimulations of the train, pooled data revealed a striking difference between the AIS group, with a mean spike number change significantly different from 0 (−22.4 ± 5.9%; P = 0.004; n = 10) and the distal group whose mean spike number change was close to 0 (0.4 ± 5.2%; P = 0.9; n = 5). These results indicate a significant inhibitory effect of photolysis in the AIS and no effect in the distal axon (Fig. 6*B*). As expected, the counts for the first 9 stimulations before photolysis did not reveal any difference between control and photolysis, either in the AIS or in distal sites

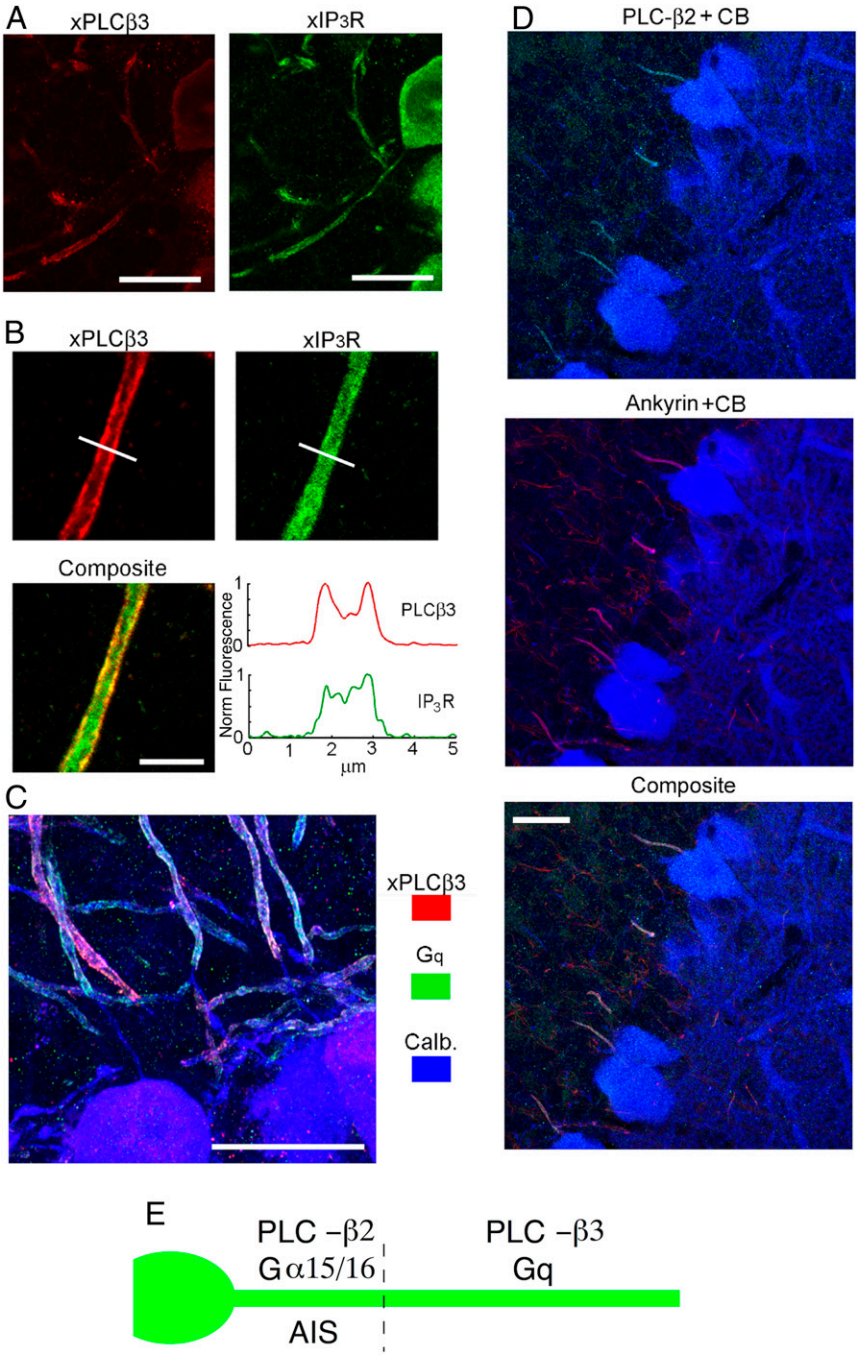

Fig. 5. Complementary expression pattern of PLC-β2 and -β3 in PC axon. (*A*) Colabeling of PLC-β3 with IP_3R. (*A*, *Left*) PLC-β3 is present in the soma and in the axon, but not in the initial segment. (*A*, *Right*) IP_3R labeling is continuous. (Scale bar, 20 μm.) (*B*) PLC-β3 is membrane localized in the axon, whereas IP_3Rs is distributed throughout the interior. Line profiles of the fluorescence intensity for the two markers (*Bottom Right*) highlight the different spatial patterns. (Scale bar, 5 μm.) (*C*) PLC-β3 and G_q exhibit a near-identical localization, both of them being excluded from the same stretch of proximal axon, in which calbindin labeling remains clearly visible. (Scale bar, 20 μm.) (*D*) Triple staining with antibodies against PLC-β2, calbindin, and ankyrin, showing that PLC-β2 is present exclusively in the initial segment where it costains with ankyrin. (Scale bar, 20 μm.) (*E*) Summary illustrating the differential localizations of $G_{\alpha 15/\alpha 16}$, G_q, PLC-β2, and PLC-β3.

(Fig. 6*B*). Because of the proximity of the AIS to the somatic compartment, we verified that Ca_i rises in these experiments were restricted to the AIS, by monitoring soma and AIS Ca_i during photolysis targeted to the AIS. In 3 experiments, whereas peak IP_3-evoked Ca_i rose in the AIS to 129 ± 31%, the somatic fluorescence showed no detectable change, as exemplified in Fig. 6*C*. Altogether, these results indicate that electrical excitability in PCs is inhibited by local IP_3 rises in the AIS. They further indicate that IP_3 exerts its inhibitory action by elevating Ca_i in the AIS, while a similar IP_3-induced Ca_i elevation further down the axon has no effect on spike generation.

To test whether IP_3 photolysis elicited a downward shift of the membrane potential, we compared the peak hyperpolarization after the AP train with and without photolysis, finding no difference (with: −83.4 ± 0.5 mV; without: −83.1 ± 0.6 mV; $P > 0.05$; paired t test among individual cell results, $n = 10$). Likewise, we found that in a resting cell, IP_3 photolysis in the AIS did not induce any detectable potential change. These results argue against a large IP_3-induced conductance change. It was reported that in PCs, inhibition of T-type voltage-gated Ca^{2+} channels (VGCCs) in the AIS leads to AP firing inhibition, accompanied by an increase in AP threshold potential (24). By contrast we found that the value of the threshold potential for AP firing was the same without (−53.15 ± 2.07 mV) and with (−53.12 ± 2.08 mV) photolysis ($P > 0.05$, $n = 10$). Therefore, the effect of IP_3 photolysis is likely not mediated by down-regulation of T-type VGCCs. Taken together these results indicate that possible IP_3-induced changes in cell membrane properties are too small to be detectable when

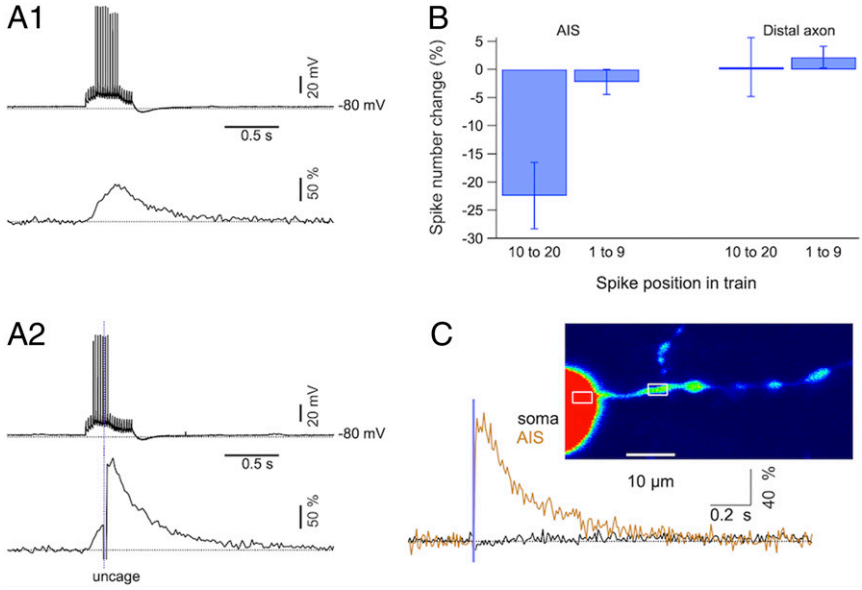

Fig. 6. IP_3 photolysis in the axon initial segment inhibits firing. (*A1*) *Upper* trace: Membrane voltage recorded under current clamp during a 50-Hz train of 20 pulses of 5-ms duration and 750-pA amplitude, leading to spikes in 10 out of the 20 pulses. *Lower* trace: Corresponding $\Delta F/F_o$ trace recorded in the AIS. (*A2*) A subsequent run in the same experiment where a photolysis pulse (1-ms duration, 2-V amplitude) was delivered to the AIS after the ninth pulse. Note the decrease in the number of spikes for the time period following the laser pulse and the larger amplitude of the Ca_i rise, which has an inflection on its rising phase corresponding to the onset of the photolysis-evoked response. (*B*) Pooled data showing percentage changes in the number of APs when applying a laser pulse (as in *A2*) compared to the number without the laser pulse (as in *A1*). For each experiment, AP numbers were analyzed in two time periods, before and after the time of the laser pulse (respectively, for spike positions 1 through 9 and for spike positions 10 through 20). Data from 15 experiments were divided in two groups depending on the location of the axonal site targeted for photolysis. The AIS group included experiments with the site located at less than 26 µm from the soma exit, whereas the distal axon group included experiments for which this distance was larger than 30 µm. Bars denote SEM. The only group that differs significantly from 0 is that of the last 11 pulses for the AIS, with Student's *t* and *P* values of −3.8 and 0.004. Corresponding values for the first 9 pulses at the AIS were −0.98 and 0.4. Values for the distal axon are 0.08 and 0.9 (last 11 pulses), and 1.1 and 0.4 (first 9 pulses). (*C*) Parallel scans over the AIS and over an equal-size somatic region, as shown in the *Top* image. A photolysis pulse (1-ms duration, 2-V amplitude) induces a Ca_i rise in the AIS (yellow) but not in the soma (black).

photoreleasing IP_3 in the AIS. This is not surprising when considering the expected value of the capacitance of the AIS membrane. Assuming an axon diameter of 2 µm, an AIS length of 28 µm, and a unitary surface capacitance of 1 µF/cm^2, the expected value for the AIS membrane capacitance is 1.8 pF, more than two orders of magnitude smaller than the input capacitance of a PC (41). Therefore, only a massive increase in the AIS conductance can be detected when using whole-cell recording.

In PCs, BK channels are potent regulators of AP firing alongside T-type VGCCs and SK channels (42, 43). Furthermore, immunostaining indicates the presence of BK channels in specific parts of PC axons, including the AIS (19). Finally, in certain cells, intracellular calcium stores regulate the gain of VGCC-BK channel coupling ("double nanodomain coupling": ref. 44); note however that such coupling has so far been shown only in the somatic compartment). Therefore, it is plausible that the micromolar Ca^{2+} concentration rises elicited by IP_3 could lead to BK or SK activation in the AIS and consequently to AP inhibition, but a direct test of this possibility must await further investigations.

Downstream Effects of IP_3 in Axon Terminals. As illustrated in Fig. 1*D*, IP_3R-I staining was clear in axonal varicosities surrounding large somata at the level of the DCN where PCs make their synaptic contacts. To search for a functional role of IP_3Rs on putative synaptic terminals, we moved from acute slices to dissociated cultures. There are two reasons for this choice. First, such a preparation lends itself to Acetoxymethyl ester (AM) loading and thus allowed us to probe synaptic transmission from synaptic terminals not suffering from washout. Second, PCs in these cultures form synapses onto DCN somata that can be easily recognized with fluorescence optics from PC-specific GFP fluorescence (Fig. 7*A*). PCs maintained in culture can lose their responses to IP_3 photolysis (45). In the present conditions, when cultures were loaded with a membrane-permeable form of caged IP_3 (*Methods*) somatic Ca_i responses to photolysis were observed in PC somata (average peak values 69 ± 7%, $n = 17$; *SI Appendix*, Fig. S4) as well as in presumptive boutons with average peak values of 37 ± 7% ($n = 9$ boutons; example in Fig. 7*B*). Miniature inhibitory postsynaptic currents (mIPSCs) recorded from DCN (Fig. 7*C*) had mean amplitudes of 49.2 ± 6.4 pA and frequencies of 16.4 ± 2.3 Hz ($n = 10$). To quantify effects of photolysis, control runs were interspersed with runs in which a photolysis pulse was delivered to release IP_3 from putative terminals. Pooled results from 10 cells (Fig. 7*D*) show that mIPSC frequency increased by a factor of 1.31 ± 0.05 ($n = 10$) on the first time bin following photolysis, while there were no discernible changes in the amplitude (mean normalized amplitude at the first time bin: 0.97 ± 0.05, $n = 10$). mIPSC frequency returned to basal levels 4 s after photolysis. Thapsigargin blocked the photolysis-evoked Ca_i rise in boutons (*SI Appendix*, Fig. S5) and the mIPSC frequency increase (Fig. 7*E*) in accord with an ER Ca^{2+} source. These experiments indicate that a local IP_3 increase in PC terminals produces a large enough Ca_i rise to induce exocytosis of synaptic vesicles.

P2Y1Rs as Candidate Activators of the IP_3 Pathway. The above results raise the question of the nature of the receptors upstream of PLC activation. In several systems including the hippocampus and cerebellum, purinergic receptors of the P2Y1R subtype are present in GABAergic axons, and activation of P2Y1Rs enhances GABA release (46, 47). In astrocytoma cells, activation of P2YIRs results in PLC activation and Ca_i elevation (48). Therefore, P2YIRs are candidate activators of the IP_3 pathway in PC axons. Immunohistological experiments revealed P2Y1Rs in the soma of PCs, in conformity to earlier findings (49). In

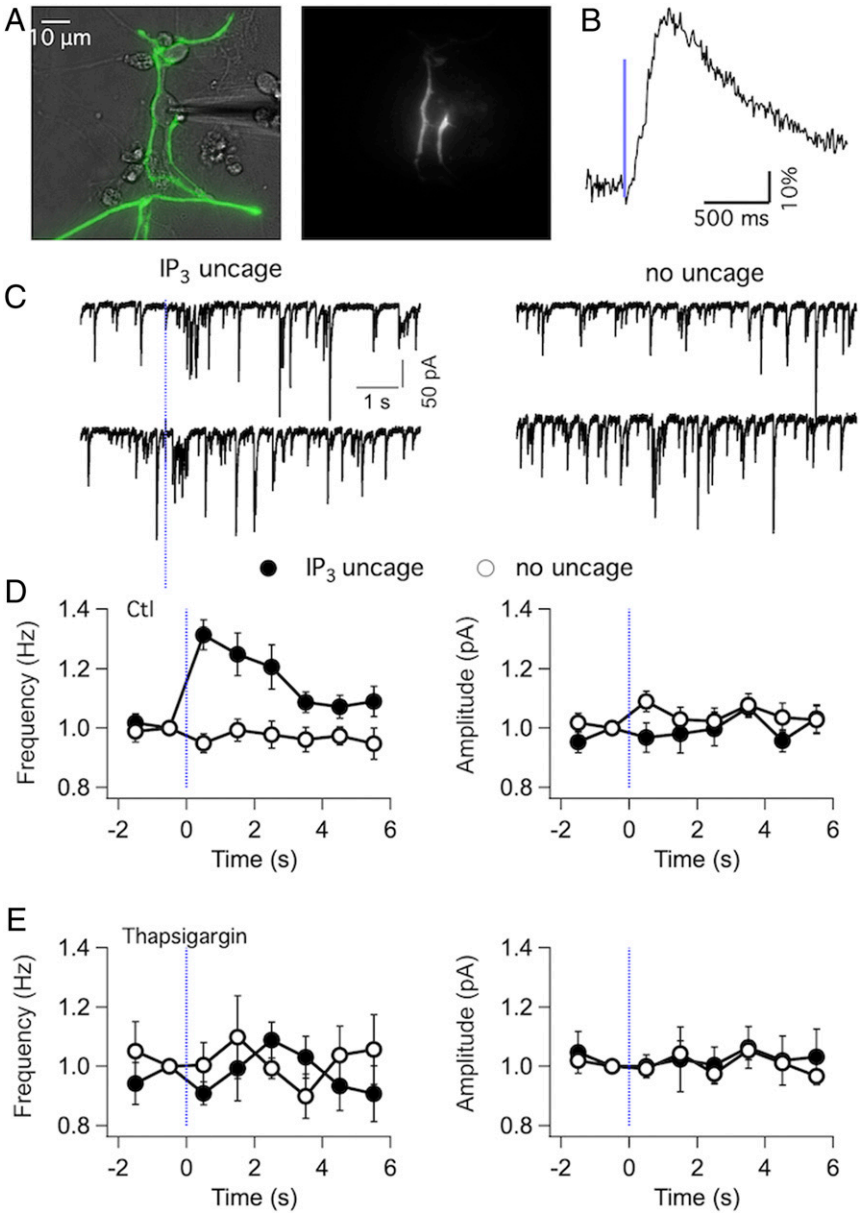

Fig. 7. IP_3 photolysis elicits GABA release from axons of cultured PCs. (*A*) Transmitted image of a DCN neuron under WCR (*Left*) and the EGFP fluorescence image upon 405-nm laser illumination (*Right*) of the same field showing the IP_3-photolysed PC terminals surrounding the patched soma. The culture was loaded with a permeable version of caged IP_3, as detailed in *Methods*. (*B*) Time course of the Ca_i rise recorded from putative boutons over DCN somata using the Ca^{2+}-sensitive protein RFP670. The photolysis pulse has 1-ms duration and 5-V amplitude. (*C*, *Left*) Two representative traces of mIPSCs, recorded at a holding potential of −70 mV. The dashed bar indicates the time of photolysis, with a pulse duration of 1 ms and amplitude of 5 V. Note increase in mIPSC frequency shortly after uncaging. (*C*, *Right*) Similar recording from the same neuron, with no photolysis performed. (*D*) mIPSC frequency (*Left*) and amplitude (*Right*) values from 10 experiments are binned over 1-s time bins and displayed as a function of time (open circles: no photolysis; closed circles: photolysis). (*E*) Corresponding analysis from six experiments where 1 µM thapsigargin was applied for 20 min prior to recording. Paired Student's *t* test was done to compare frequency and amplitude values for control versus photolysis runs in the first time bin after photolysis in *D* and *E*. Frequency for the experiments summarized in *D*, *Left* showed a significant difference, with *t* and *P* values of 4.0 and 0.003, indicating IP_3-induced GABA release. By contrast, no statistical difference was present for the amplitude values in test experiments (*D*, *Right*), nor for frequency or amplitude values in thapsigargin experiments (*E*).

addition, we found P2Y1Rs in the AIS. Remarkably, P2YIR staining stopped abruptly together with ankyrin staining, indicating an exact restriction to the AIS membrane (Fig. 8 *A*, *Upper* row). In addition, we found P2Y1Rs in calbindin-positive axon terminals surrounding large somata of deep cerebellar nuclei (Fig. 8 *A*, *Lower* row). Both in the AIS and in terminals, P2Y1Rs were closely associated with Gα15/16 and with PLC-β2 (*SI Appendix*, Fig. S6). Therefore, we propose that P2Y1Rs are the receptors upstream of the Gα15/PLC-β2 pathway. To test this hypothesis, we performed puffer applications of the specific P2Y1R agonist MRS 2365 (50) to PCs in the presence of tetrodotoxin (TTX). Preliminary experiments using whole-cell recording revealed only small amplitude, poorly reproducible Ca^{2+} concentration increases in response to local MRS 2365 applications (up to 1 mM in puffer pipette, 10-s-long applications; *SI Appendix*, Fig. S7). However, whole-cell recording may have led to the loss of functionally important diffusible factors of the Ca^{2+}-producing pathway, as previously shown for such a

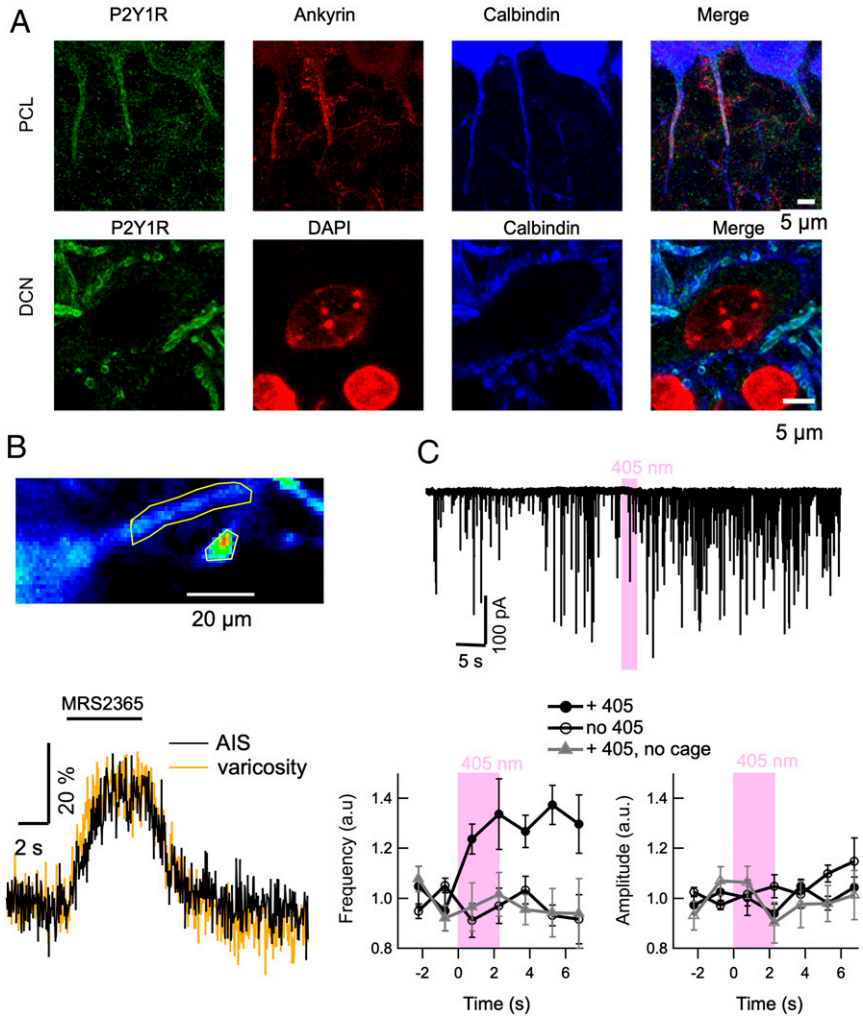

Fig. 8. Sensitivity of AIS and DCN terminals to purinergic agonists. (*A*, *Upper*) In the PC layer, staining for the purinergic receptor P2Y1R (green) coincides with that for ankyrin G in AIS regions of PCs (red). (*A*, *Lower*) P2Y1R staining in terminals surrounding DCN principal neurons. (*B*) In GCaMP6f-expressing PCs in acute slices, local pressure application of the specific P2Y1R agonist MRS 2365 (100 µM in puffer pipette) in the AIS elicits a Ca_i response both in the AIS (black) and in a presumptive presynaptic terminal (yellow). (*C*) Recordings from DCN somata in dissociated cultures. (*C*, *Upper*) ATP uncaging (pink bar above current trace) elicits prolonged increase in miniature IPSC frequency. (*C*, *Lower*) Summary data ($n = 6$) showing that ATP uncaging increases mIPSC frequency (t and P values of −4.2 and 0.008) but does not change mIPSC mean amplitude. Gray triangles correspond to average values from five experiments using the same laser protocol at twice the power, but with no cage present in the extracellular solution. There was no effect on either frequency or amplitude.

pathway in other systems (51). To avoid washout of cell constituents, we performed additional experiments using the GCaMP6F × L7Cre mouse line, where PCs specifically express the Ca^{2+}-sensitive protein GCaMP6f. Under these conditions, local MRS 2365 applications led to Ca_i elevations in the AIS (Fig. 8*B*; mean response to 5-s-long puffer applications using 100 µM MRS 2365 in puffer pipette: 21.4 ± 4.5%, seven cells) and in presumptive presynaptic terminals (Fig. 8*B*). To test further the effects of P2Y1R activation in presynaptic terminals, we performed local ATP uncaging onto PC terminals contacting DCN somata in dissociated cultures in the presence of TTX, while recording from the postsynaptic DCN somata. We found a marked increase in miniature current frequency (ratio to control: 1.34 ± 0.14, six cells), and no change in miniature current amplitude (ratio to control: 0.94 ± 0.04, compare filled and empty circles in Fig. 8*C*). As a control for laser damage, 405-nm illumination performed at twice the power, but in the absence of cage, had no effect on mIPSCs (gray triangles in Fig. 8*C*). Altogether, these results indicate that P2YIRs are placed upstream of the Gα15/PLC-β2 pathway both in the AIS and in presynaptic terminals, that their activation leads to Ca_i rises, and that in presynaptic terminals, these Ca_i rises lead to GABA release.

Discussion

This work shows that in PC axons, photorelease of caged IP_3 leads to substantial Ca_i rises. This is a demonstration of functional axonal IP_3Rs in central neurons. Our results also reveal the presence of two distinct IP_3-producing signaling cascades, one in the AIS and in synaptic terminals, and one in the rest of the axon. They further show that IP_3 elevation in the AIS inhibits AP firing, whereas IP_3 elevation in axon terminals results in GABA release. Finally, we find that purinergic agonists engage the IP_3 pathway both in the AIS and in terminals, likely through activation of P2Y1Rs. Altogether these results suggest potent roles of IP_3R-linked signaling pathways in controlling several axon functions.

Characteristics of IP_3R-Induced Axonal Ca_i Rises. The characteristics of IP_3R-induced axonal Ca_i rises are similar to those previously obtained for somatodendritic IP_3 photolysis (26, 52, 53). Compared to IP_3Rs in astrocytes and in peripheral tissue, those in

PCs have a low affinity and rapid kinetics, leading to maximal Ca_i responses that are characterized by a rapid onset and a large amplitude (52). Consistent with earlier findings in PC dendrites, we find responses with rise times of <100 ms when using strong laser intensity (Fig. 3). Our experiments with a low-affinity calcium indicator indicate peak Ca_i levels reaching >5 μM, a value consistent with those previously estimated for dendritic PC responses (26). Such large maximal responses are in line with our finding of an IP_3-dependent increase in transmitter release (Fig. 7).

Another key finding is that IP_3R-induced Ca_i transients are sharply confined near the site of IP_3 photolysis in the axon. Our results (Fig. 3) indicate a rapid falloff of response amplitude over distances of a few micrometers, consistent with a purely diffusive process of Ca_i spread from a point source. Likewise, RyRs-dependent axonal Ca_i signals found in cerebellar molecular layer interneurons, called SCaTs (for spontaneous calcium transients), decline sharply with distance (2). Also, previous results using local IP_3 photolysis in PC dendrites indicate strictly localized responses (53). By contrast, in dendrites of hippocampal pyramidal neurons, activation of metabotropic glutamate receptors (mGluRs) results in IP_3R-dependent, back-propagating Ca^{2+} waves (54). The lack of spread of Ca_i signals originating from intracellular Ca^{2+} stores in molecular layer interneurons (MLIs) and PCs may be explained on the basis of the high internal Ca^{2+} buffering in these cells, notably due to the presence of large concentrations of parvalbumin in MLIs (55), and of parvalbumin and calbindin in PCs (56). An important implication of the local nature of IP_3 signaling in PC axons is that the function of IP_3Rs is presumably diverse, depending on the nature of the axonal structure harboring the IP_3Rs. Our finding of IP_3R-induced Ca_i rises in various axonal structures, including the AIS, smooth axon stretches, branch points, varicosities, and presynaptic nerve endings (Fig. 2), raises the possibility that IP_3 may have specific local roles in each of these structures. While our present results suggest different functional roles of IP_3 in the AIS and in presynaptic nerve endings, as further discussed below, the possibility of still other functions of IP_3Rs located in different axon structures must be kept open.

Two Spatially Segregated IP_3R-Linked Signaling Pathways in PC Axons. A remarkable finding of the present work is the identification of two distinct PLC pathways and their spatial segregation along the PC axon. A first pathway involves the metabotropic purinergic receptor P2Y1R, the GTP binding protein Gα16, and PLC-β2. This combination is found in the AIS as well as in synaptic terminals onto deep cerebellar nuclei. The second pathway involves the GTP binding protein Gq/α11, and PLC-β3; it occurs in intermediate parts of the axon. The corresponding receptor, if it exists, remains to be identified.

The two pathways are sharply delimited in space. This can be seen clearly at the boundary between the AIS and the more distal part of the axon. While P2Y1R, Gα16, and PLC-β2 stainings all stop exactly together with that of ankyrin G, at the end of the AIS, Gq/α11 and PLC-β3 stainings start immediately after the end of the AIS, and they cover the main part of the axon.

P2Y1Rs are well known to be associated to PLC activation (48); however, the exact nature of the linking G protein and of the PLC remains unclear, particularly in the nervous system. Our finding of P2Y1Rs in the AIS is consistent with earlier findings that in hippocampal cultures, P2Y1Rs regulate ankyrin G expression in the AIS (57). On the other hand, our finding of P2Y1Rs in PC terminals is consistent with earlier reports suggesting that P2Y1R activation elicits an enhancement of GABA release in hippocampal and cerebellar GABAergic axons (46, 47). These earlier studies suggest that the present signaling pathway going from P2Y1Rs to neurotransmitter release is not restricted to PCs, and may occur in several neuron types in the mammalian brain.

IP_3R-Induced Ca_i Rise and Excitability. Previous work has shown that in PCs, as in other neurons, the AIS is the site of AP initiation (12, 58, 59). It is also well established that the AIS membrane in PCs contains a high density of VGCCs, and that activation of these VGCCs leads to substantial local Ca_i elevations in response to repetitive AP discharges (18, 24). Our present results show that in addition or in complement to VGCCs, IP_3 receptors control the local Ca_i in PC AIS, and that their activation inhibits AP discharge. Furthermore, we propose here a coherent signaling cascade in the AIS involving the sequential activation of P2Y1R, Gα16, and PLC-β2, and leading to IP_3 production and Ca^{2+} release. Together with previous results on VGCCs, the present results suggest that the Ca_i level at the AIS is a regulator of AP discharge and that this level is the target of at least two different signaling cascades.

Our results showing calcium rises in the AIS as a result of P2Y1R activation suggest that ATP, or possibly ADP, is the signal commanding the IP_3 cascade in the AIS. In PCs, the AIS is encapsulated by a dense structure called pinceau, formed by endings of basket cell axons. ATP could accumulate in the space comprised between the pinceau and the PC axon following AP-induced corelease of ATP and GABA from basket terminals. Since astrocytes are closely associated with the AIS in PCs (60), and since pinceau membranes are rich in voltage-dependent K^+ channels (61, 62), it is also possible that, following presynaptic firing of basket cells, the K^+ concentration increases in the pinceau-covered region, inducing ATP release from astrocytes associated with the AIS (61). By either mechanism, ATP-induced AIS signals could contribute to enhancing the inhibition exerted by basket cells on PC firing.

IP_3R-Induced Ca_i Rise and Transmitter Release. The present work shows that IP_3 photolysis in PC synaptic terminals is able to elicit GABA release onto DCN neurons by recruiting Ca^{2+} release from the ER. This finding confirms and extends previous evidence indicating a contribution of ER-mediated Ca^{2+} release to synaptic transmission. Previous pharmacological studies on cerebellum and hippocampus revealed the sensitivity of miniature synaptic current frequency (2, 4, 63, 64) and evoked synaptic currents (65) to drugs affecting CICR. Additionally, in hippocampal terminals, Ca^{2+} influx through presynaptic nicotinic ACh receptors potently engages CICR, leading to massive neurotransmitter release (66). A similar recruitment of presynaptic Ca^{2+} stores was subsequently demonstrated in retinal terminals following activation of presynaptic Ca^{2+}-permeant AMPA receptors (67) and in cerebellar interneuron terminals following activation of either presynaptic Ca^{2+}-permeant AMPA receptors (68) or presynaptic NMDA receptors (69).

As in the AIS, our results suggest ATP, or possibly ADP, as the trigger of the IP_3 cascade in DCN terminals. And as in the AIS, likely sources of ATP are on one hand corelease of ATP with another neurotransmitter, following presynaptic release, and on the other hand, activation of astrocytes. In conclusion, our work suggests that in PCs, axonal IP_3Rs are involved in two distinct integrated signaling pathways; it further suggests that one of these pathways can alter PC output on a time scale of seconds, and that this may be driven by local neuronal and/or glial activity.

Methods

All experimental procedures were designed in accordance with animal care guidelines of the host institution. They were approved by the ethical committee of Paris Descartes University and by the "Prefecture de Police," in agreement with European Directive 86/609/EEC. Experiments were performed in acute cerebellar slices from Wistar rats and C57bl6 mice of either gender, aged 12 to 33 and in primary cultures of rat cerebellar following procedures detailed in *SI Appendix*. Details on confocal imaging of immunostained preparations and on the primary and secondary antibodies used are provided in *SI Appendix*.

Patch-Clamp Recording, Photolysis, and 2PLSM Imaging in Slices. Tight seal WCRs were performed from PCs from slices perfused with bicarbonate-buffered saline (BBS; in mM: 125 NaCl, 2.5 KCl, 1.25 NaH_2PO_4, 25 $NaHCO_3$, 2 $CaCl_2$, 1 $MgCl_2$, and 10 glucose) at a rate of 1.2 to 1.5 ml/min while maintaining the temperature at 35 to 36 °C. For imaging and photolysis experiments the intracellular solution contained (in mM): 140 K gluconate, 5.4 KCl, 4.1 $MgCl_2$, 9.9 Hepes-K, 0.36 Na-GTP and 3.6 Na-ATP, 30 μM Alexa 594, 100 μM of the Ca^{2+}-sensitive indicator OGB1 and 400 μM D-myo-Inositol 1,4,5-triphosphate, P4(5)-(1-(2-nitrophenyl)ethyl) ester, tris(triethylammonium) salt (NPE-caged IP_3). Fluorophores and caged IP_3 were purchased from Invitrogen. Uncompensated access resistance values were 4 to 10 MΩ during recording. A 60 to 70% series-resistance compensation was applied.

Photolysis was achieved with a 405-nm laser (Obis 405-nm laser, Coherent), coupled to the side port of an Axioexaminer Zeiss microscope by an optical fiber. Estimates of beam parameters were obtained by imaging the reflection of the 405-nm beam focused on a silver mirror, as detailed in ref. 25. The beam projection for the *z* level giving maximal intensity was well described by a Gaussian distribution with a full width at half maximum (FWHM) of 350 nm. Along the *z* axis the distribution was wider, with a FWHM of 8.6 μm. Laser pulses had 1- to 4-ms durations and 0.5- to 2-V amplitudes, corresponding to 2 to 8 mW out of the 63× objective.

To estimate the IP_3 concentration achieved by axonal uncaging, we calibrated the response using vesicles loaded with NPE-HPTS [the 1-(2-nitrophenyl)ethyl ether of pyranine], a fluorescent version of the cage (70). This calibration indicated that a 1 ms*V power, corresponding to the apparent half maximum calcium response, was able to release 148 μM IP_3. After correction for light absorption in the tissue (25), the corresponding number was 44 μM.

To assess effects of IP_3 photolysis on different axonal sites, PCs were kept in voltage clamp with a holding potential of −70 mV. Fluorescence was recorded from axonal regions using a custom-built two-photon system based on the design in ref. 71, with 820-nm excitation provided by a MaiTai Ti-Sapphire laser (Spectra Physics). Raster scans of 10 × 10 μm regions encompassing the selected site were performed at dwell times of 18 ms with average power at the objective back pupil kept under 8 mW. To analyze the spread of fluorescence signals, a "multiple patch scan" version of raster scanning was used, allowing for sequential scanning of three to four nonadjacent 5 × 5 μm regions of the axon at a dwell time of 17 to 20 ms (example in Fig. 3). Fluorescence changes were analyzed in the pixels encompassing the sites relative to prestimulus values with software written in the IGOR-Pro programming environment (Wavemetric). Changes are expressed in %, as $\Delta F/F_o = 100*(F-F_o)/(F_o-B)$, where F is the measured fluorescence signal at any given time, F_o the average from the prestimulus period, and B the average value, at each time point, of the background fluorescence from four regions of the imaged field which do not contain any part of the dye-filled cell.

To assess effects of IP_3 photolysis on spike generation, PCs were recorded under current clamp. A steady hyperpolarizing current was applied to maintain the holding membrane potential between −77 mV and −79 mV, a level sufficiently negative to prevent spontaneous spiking. Trains (20× at 50 Hz) of depolarizing current steps (5-ms duration) were delivered at 1-min intervals. Current step amplitude was selected to induce an AP in ∼35 to 45% of the cases. Voltage changes due to the flow of current in the pipette resistance were <5 mV and were left uncorrected. We interspersed test runs in which a photolysis pulse was delivered after the ninth step in the train, with control runs in which no photolysis was performed. We defined the "spike number change" as the number of spikes in runs with no photolysis minus the number of spikes in runs with photolysis, divided by the number of spikes in runs without photolysis. We computed this spike number change separately for the first 9 steps (where no significant difference was expected) and for the last 11 steps (where IP_3-linked differences should be apparent) in the train. Values were averaged over five to seven repetitions in each experiment.

To search for activation of P2Y1Rs in nondialyzed PCs, we prepared cerebellar slices from mice obtained by crossing the L7 Cre line with the TIGRE 2.0 GCaMP6f reporter line (72), which express the genetically encoded calcium protein GCaMP6f selectively in PCs. The excitation wavelength of the MaiTai laser was set at 910 nm and average power at the objective back pupil was kept under 15 mW. The P2Y1R agonist 1′*S*,2′*R*,3′*S*,4′*R*,5′*S*)-4-[(6-amino-2-methylthio-9*H*-purin-9-yl)-1-diphosphoryloxymethyl]bicyclo[3.1.0]hexane-2,3-diol; 2MeSADP, 2-methylthio-ADP; MRS2179, N_6-methyl 2′-deoxyadenosine-3′,5′-bisphosphate (MRS 2365) was applied locally by a pressure-controlled puffer pipette (internal diameter 2 to 2.5 μm).

Patch-Clamp Recording and Photolysis in Deep Cerebellar Nuclei. To study the effects of photolysis on mIPSCs, cerebellar cultures (*SI Appendix*) were maintained at room temperature in an external solution containing (in mM): 145 NaCl, 5 KOH, 2 $CaCl_2$, 1 $MgCl_2$, 10 Hepes, and 10 glucose (pH 7.3). WCR was performed with a pipette solution containing (in mM): 155 CsCl, 0.5 ethylene glycol bis (β-aminoethylether) N,N,N′,N′-tetraacetic acid (EGTA), 10 Hepes, 2 Mg-ATP, and 0.2 Na-GTP. Cultures were loaded with the membrane-permeable form of caged IP_3 (cag-iso-2-145, Sychem), prepared in 10% DMSO at a concentration of 1 mM and diluted to final concentration of 2 μM. To monitor changes in Ca_i, cultures of 1 μM Oregon Green 488 BAPTA-1 AM (Invitrogen) were added to the loading solution. The cultures were incubated for 30 to 35 min at room temperature and washed several times before transfer to the recording chamber.

DCN cells were identified by PC-specific EGFP or RFP670 fluorescence. To study effects of IP_3 photolysis on mIPSCs, DCN neurons were held at −70 mV and spontaneous synaptic currents were recorded in the presence of tetrodotoxin (1 μM) and 2,3-dioxo-6-nitro-7-sulfamoyl-benzo[f]quinoxaline (NBQX) (10 μM). A total of 6 to 20 runs of 8-s duration were acquired from each cell; runs containing photolysis pulses alternated with control runs. Off-line event analysis was performed with Igor software using the Tarotool plug-in (https://sites.google.com/site/tarotoolsregister/) to extract values for mIPSC amplitudes and frequency for 1-s bins in each run. Results were averaged over control and photolysis-containing runs. Photolysis was performed with the same system described for slices except that the 405-nm laser spot size was enlarged to a diameter of ∼25 μm in order to photolyse a large number of boutons surrounding the patched neuron (Fig. 7). Laser pulses had 1-ms duration and 5-V amplitude. In a subset of experiments, thapsigargin (1 μM) was applied for ∼30 min before recordings.

ATP uncaging experiments were carried out at near physiological temperature (34 °C). The ATP cage NPE-ATP (100 μM) was included in the bath solution. A laser spot (405 nm, 2-μm diameter, 3.5-mW intensity) was scanned for a total duration of 2.2 s over an area of 100-μm radius encompassing the recorded DCN neuron, in order to stimulate presynaptic boutons.

Statistical Analysis. Values for pooled data are given as mean ± SEM. All statistical comparisons are based on Student's *t* test and *t* and *P* values are reported for each comparison.

Data are available upon request from the corresponding author.

ACKNOWLEDGMENTS. This work was supported by a European Research Council grant to A.M. (single site, 294509), the Japan Society for the Promotion of Science (Core-to-Core Program A, Advanced Research Networks; KAKENHI grants 19H04750 and 18H02527 to S.-y.K.), the Takeda Science Foundation, and the Naito Foundation.

1. R. Bouchard, R. Pattarini, J. D. Geiger, Presence and functional significance of presynaptic ryanodine receptors. *Prog. Neurobiol.* **69**, 391–418 (2003).
2. I. Llano *et al*., Presynaptic calcium stores underlie large-amplitude miniature IPSCs and spontaneous calcium transients. *Nat. Neurosci.* **3**, 1256–1265 (2000).
3. R. Conti, Y. P. Tan, I. Llano, Action potential-evoked and ryanodine-sensitive spontaneous Ca2+ transients at the presynaptic terminal of a developing CNS inhibitory synapse. *J. Neurosci.* **24**, 6946–6957 (2004).
4. N. J. Emptage, C. A. Reid, A. Fine, Calcium stores in hippocampal synaptic boutons mediate short-term plasticity, store-operated Ca2+ entry, and spontaneous transmitter release. *Neuron* **29**, 197–208 (2001).
5. J. de Juan-Sanz *et al*., Axonal endoplasmic reticulum Ca2+ content controls release probability in CNS nerve terminals. *Neuron* **93**, 867–881.e6 (2017).
6. A. Verkhratsky, Physiology and pathophysiology of the calcium store in the endoplasmic reticulum of neurons. *Physiol. Rev.* **85**, 201–279 (2005).
7. M. J. Berridge, The endoplasmic reticulum: A multifunctional signaling organelle. *Cell Calcium* **32**, 235–249 (2002).
8. K. Kitamura, M. Kano, Dendritic calcium signaling in cerebellar Purkinje cell. *Neural Netw.* **47**, 11–17 (2013).
9. O. H. Petersen, A. V. Tepikin, Polarized calcium signaling in exocrine gland cells. *Annu. Rev. Physiol.* **70**, 273–299 (2008).
10. A. C. Horton, M. D. Ehlers, Neuronal polarity and trafficking. *Neuron* **40**, 277–295 (2003).
11. D. Debanne, Information processing in the axon. *Nat. Rev. Neurosci.* **5**, 304–316 (2004).
12. M. H. P. Kole, G. J. Stuart, Signal processing in the axon initial segment. *Neuron* **73**, 235–247 (2012).
13. C. Y.-M. Huang, M. N. Rasband, Axon initial segments: Structure, function, and disease. *Ann. N. Y. Acad. Sci.* **1420**, 46–61 (2018).
14. E. A. Finch, G. J. Augustine, Local calcium signalling by inositol-1,4,5-trisphosphate in Purkinje cell dendrites. *Nature* **396**, 753–756 (1998).
15. H. Takechi, J. Eilers, A. Konnerth, A new class of synaptic response involving calcium release in dendritic spines. *Nature* **396**, 757–760 (1998).

16. C. R. Rose, A. Konnerth, Stores not just for storage. Intracellular calcium release and synaptic plasticity. *Neuron* **31**, 519–522 (2001).
17. M. A. Dent, G. Raisman, F. A. Lai, Expression of type 1 inositol 1,4,5-trisphosphate receptor during axogenesis and synaptic contact in the central and peripheral nervous system of developing rat. *Development* **122**, 1029–1039 (1996).
18. G. Callewaert, J. Eilers, A. Konnerth, Axonal calcium entry during fast 'sodium' action potentials in rat cerebellar Purkinje neurones. *J. Physiol.* **495**, 641–647 (1996).
19. M. Hirono *et al*., BK channels localize to the paranodal junction and regulate action potentials in myelinated axons of cerebellar Purkinje cells. *J. Neurosci.* **35**, 7082–7094 (2015).
20. J. Gründemann, B. A. Clark, Calcium-activated potassium channels at nodes of Ranvier secure axonal spike propagation. *Cell Rep.* **12**, 1715–1722 (2015).
21. D. Orduz, I. Llano, Recurrent axon collaterals underlie facilitating synapses between cerebellar Purkinje cells. *Proc. Natl. Acad. Sci. U.S.A.* **104**, 17831–17836 (2007).
22. F. Díaz-Rojas, T. Sakaba, S.-Y. Kawaguchi, Ca(2+) current facilitation determines short-term facilitation at inhibitory synapses between cerebellar Purkinje cells. *J. Physiol.* **593**, 4889–4904 (2015).
23. L. Witter, S. Rudolph, R. T. Pressler, S. I. Lahlaf, W. G. Regehr, Purkinje cell collaterals enable output signals from the cerebellar cortex to feed back to Purkinje cells and interneurons. *Neuron* **91**, 312–319 (2016).
24. K. J. Bender, L. O. Trussell, Axon initial segment Ca2+ channels influence action potential generation and timing. *Neuron* **61**, 259–271 (2009).
25. F. F. Trigo, J. E. T. Corrie, D. Ogden, Laser photolysis of caged compounds at 405 nm: Photochemical advantages, localisation, phototoxicity and methods for calibration. *J. Neurosci. Methods* **180**, 9–21 (2009).
26. K. Khodakhah, D. Ogden, Fast activation and inactivation of inositol trisphosphate-evoked Ca2+ release in rat cerebellar Purkinje neurones. *J. Physiol.* **487**, 343–358 (1995).
27. J. Hirota, H. Ando, K. Hamada, K. Mikoshiba, Carbonic anhydrase-related protein is a novel binding protein for inositol 1,4,5-trisphosphate receptor type 1. *Biochem. J.* **372**, 435–441 (2003).
28. K. Khodakhah, C. M. Armstrong, Inositol trisphosphate and ryanodine receptors share a common functional Ca2+ pool in cerebellar Purkinje neurons. *Biophys. J.* **73**, 3349–3357 (1997).
29. S. Nomura, M. Fukaya, T. Tsujioka, D. Wu, M. Watanabe, Phospholipase Cbeta3 is distributed in both somatodendritic and axonal compartments and localized around perisynapse and smooth endoplasmic reticulum in mouse Purkinje cell subsets. *Eur. J. Neurosci.* **25**, 659–672 (2007).
30. Z. Kouchi *et al*., Phospholipase Cdelta3 regulates RhoA/Rho kinase signaling and neurite outgrowth. *J. Biol. Chem.* **286**, 8459–8471 (2011).
31. J.-I. Hwang *et al*., Molecular cloning and characterization of a novel phospholipase C, PLC-η. *Biochem. J.* **389**, 181–186 (2005).
32. J. K. Kim *et al*., Phospholipase C-η1 is activated by intracellular Ca(2+) mobilization and enhances GPCRs/PLC/Ca(2+) signaling. *Cell. Signal.* **23**, 1022–1029 (2011).
33. C. H. Lee, D. Park, D. Wu, S. G. Rhee, M. I. Simon, Members of the Gq α subunit gene family activate phospholipase C β isozymes. *J. Biol. Chem.* **267**, 16044–16047 (1992).
34. D. Wu, A. Katz, M. I. Simon, Activation of phospholipase C β 2 by the α and β γ subunits of trimeric GTP-binding protein. *Proc. Natl. Acad. Sci. U.S.A.* **90**, 5297–5301 (1993).
35. T. Kozasa *et al*., Purification and characterization of recombinant G16 alpha from Sf9 cells: Activation of purified phospholipase C isozymes by G-protein alpha subunits. *Proc. Natl. Acad. Sci. U.S.A.* **90**, 9176–9180 (1993).
36. H. Jiang, D. Wu, M. I. Simon, Activation of phospholipase C β 4 by heterotrimeric GTP-binding proteins. *J. Biol. Chem.* **269**, 7593–7596 (1994).
37. T. M. Wilkie, P. A. Scherle, M. P. Strathmann, V. Z. Slepak, M. I. Simon, Characterization of G-protein α subunits in the Gq class: Expression in murine tissues and in stromal and hematopoietic cell lines. *Proc. Natl. Acad. Sci. U.S.A.* **88**, 10049–10053 (1991).
38. S. M. Jenkins, V. Bennett, Ankyrin-G coordinates assembly of the spectrin-based membrane skeleton, voltage-gated sodium channels, and L1 CAMs at Purkinje neuron initial segments. *J. Cell Biol.* **155**, 739–746 (2001).
39. M. Watanabe *et al*., Patterns of expression for the mRNA corresponding to the four isoforms of phospholipase Cbeta in mouse brain. *Eur. J. Neurosci.* **10**, 2016–2025 (1998).
40. M. Montaña *et al*., Cellular neurochemical characterization and subcellular localization of phospholipase C β1 in rat brain. *Neuroscience* **222**, 239–268 (2012).
41. I. Llano, A. Marty, C. M. Armstrong, A. Konnerth, Synaptic- and agonist-induced excitatory currents of Purkinje cells in rat cerebellar slices. *J. Physiol.* **434**, 183–213 (1991).
42. A. M. Swensen, B. P. Bean, Ionic mechanisms of burst firing in dissociated Purkinje neurons. *J. Neurosci.* **23**, 9650–9663 (2003).
43. M. D. Womack, C. Chevez, K. Khodakhah, Calcium-activated potassium channels are selectively coupled to P/Q-type calcium channels in cerebellar Purkinje neurons. *J. Neurosci.* **24**, 8818–8822 (2004).
44. T. Irie, L. O. Trussell, Double-nanodomain coupling of calcium channels, ryanodine receptors, and BK channels controls the generation of burst firing. *Neuron* **96**, 856–870.e4 (2017).
45. M. D. Womack, J. W. Walker, K. Khodakhah, Impaired calcium release in cerebellar Purkinje neurons maintained in culture. *J. Gen. Physiol.* **115**, 339–346 (2000).
46. D. N. Bowser, B. S. Khakh, ATP excites interneurons and astrocytes to increase synaptic inhibition in neuronal networks. *J. Neurosci.* **24**, 8606–8620 (2004).
47. F. Saitow, T. Murakoshi, H. Suzuki, S. Konishi, Metabotropic P2Y purinoceptor-mediated presynaptic and postsynaptic enhancement of cerebellar GABAergic transmission. *J. Neurosci.* **25**, 2108–2116 (2005).
48. T. M. Filtz, Q. Li, J. L. Boyer, R. A. Nicholas, T. K. Harden, Expression of a cloned P2Y purinergic receptor that couples to phospholipase C. *Mol. Pharmacol.* **46**, 8–14 (1994).
49. M. J. Morán-Jiménez, C. Matute, Immunohistochemical localization of the P2Y(1) purinergic receptor in neurons and glial cells of the central nervous system. *Brain Res. Mol. Brain Res.* **78**, 50–58 (2000).
50. R. G. Ravi *et al*., Adenine nucleotide analogues locked in a Northern methanocarba conformation: Enhanced stability and potency as P2Y(1) receptor agonists. *J. Med. Chem.* **45**, 2090–2100 (2002).
51. R. Horn, A. Marty, Muscarinic activation of ionic currents measured by a new whole-cell recording method. *J. Gen. Physiol.* **92**, 145–159 (1988).
52. K. Khodakhah, D. Ogden, Functional heterogeneity of calcium release by inositol trisphosphate in single Purkinje neurones, cultured cerebellar astrocytes, and peripheral tissues. *Proc. Natl. Acad. Sci. U.S.A.* **90**, 4976–4980 (1993).
53. D. V. Sarkisov, S. E. Gelber, J. W. Walker, S. S.-H. Wang, Synapse specificity of calcium release probed by chemical two-photon uncaging of inositol 1,4,5-trisphosphate. *J. Biol. Chem.* **282**, 25517–25526 (2007).
54. T. Nakamura *et al*., Inositol 1,4,5-trisphosphate (IP3)-mediated Ca2+ release evoked by metabotropic agonists and backpropagating action potentials in hippocampal CA1 pyramidal neurons. *J. Neurosci.* **20**, 8365–8376 (2000).
55. T. Collin *et al*., Developmental changes in parvalbumin regulate presynaptic Ca2+ signaling. *J. Neurosci.* **25**, 96–107 (2005).
56. L. Fierro, I. Llano, High endogenous calcium buffering in Purkinje cells from rat cerebellar slices. *J. Physiol.* **496**, 617–625 (1996).
57. W. Zhang, A. Bonadiman, M. Ciorraga, M. J. Benitez, J. J. Garrido, P2Y1 purinergic receptors modulate axon initial segment initial development. *Front. Cell. Neurosci.* **13**, 152 (2019).
58. Z. M. Khaliq, I. M. Raman, Relative contributions of axonal and somatic Na channels to action potential initiation in cerebellar Purkinje neurons. *J. Neurosci.* **26**, 1935–1944 (2006).
59. A. Foust, M. Popovic, D. Zecevic, D. A. McCormick, Action potentials initiate in the axon initial segment and propagate through axon collaterals reliably in cerebellar Purkinje neurons. *J. Neurosci.* **30**, 6891–6902 (2010).
60. C. Sotelo, Development of "Pinceaux" formations and dendritic translocation of climbing fibers during the acquisition of the balance between glutamatergic and gamma-aminobutyric acidergic inputs in developing Purkinje cells. *J. Comp. Neurol.* **506**, 240–262 (2008).
61. M. Bobik, M. H. Ellisman, B. Rudy, M. E. Martone, Potassium channel subunit Kv3.2 and the water channel aquaporin-4 are selectively localized to cerebellar pinceau. *Brain Res.* **1026**, 168–178 (2004).
62. M. J. Kole *et al*., Selective loss of presynaptic potassium channel clusters at the cerebellar basket cell terminal pinceau in Adam11 mutants reveals their role in ephaptic control of Purkinje cell firing. *J. Neurosci.* **35**, 11433–11444 (2015).
63. N. Savić, M. Sciancalepore, Intracellular calcium stores modulate miniature GABA-mediated synaptic currents in neonatal rat hippocampal neurons. *Eur. J. Neurosci.* **10**, 3379–3386 (1998).
64. C. R. L. Simkus, C. Stricker, The contribution of intracellular calcium stores to mEPSCs recorded in layer II neurones of rat barrel cortex. *J. Physiol.* **545**, 521–535 (2002).
65. M. Galante, A. Marty, Presynaptic ryanodine-sensitive calcium stores contribute to evoked neurotransmitter release at the basket cell-Purkinje cell synapse. *J. Neurosci.* **23**, 11229–11234 (2003).
66. G. Sharma, S. Vijayaraghavan, Modulation of presynaptic store calcium induces release of glutamate and postsynaptic firing. *Neuron* **38**, 929–939 (2003).
67. A. E. Chávez, J. H. Singer, J. S. Diamond, Fast neurotransmitter release triggered by Ca influx through AMPA-type glutamate receptors. *Nature* **443**, 705–708 (2006).
68. B. Rossi, G. Maton, T. Collin, Calcium-permeable presynaptic AMPA receptors in cerebellar molecular layer interneurones. *J. Physiol.* **586**, 5129–5145 (2008).
69. B. Rossi *et al*., Current and calcium responses to local activation of axonal NMDA receptors in developing cerebellar molecular layer interneurons. *PLoS One* **7**, e39983 (2012).
70. M. Canepari, L. Nelson, G. Papageorgiou, J. E. Corrie, D. Ogden, Photochemical and pharmacological evaluation of 7-nitroindolinyl-and 4-methoxy-7-nitroindolinyl-amino acids as novel, fast caged neurotransmitters. *J. Neurosci. Methods* **112**, 29–42 (2001).
71. Y. P. Tan, I. Llano, A. Hopt, F. Würriehausen, E. Neher, Fast scanning and efficient photodetection in a simple two-photon microscope. *J. Neurosci. Methods* **92**, 123–135 (1999).
72. T. L. Daigle *et al*., A suite of transgenic driver and reporter mouse lines with enhanced brain-cell-type targeting and functionality. *Cell* **174**, 465–480.e22 (2018).